University of Groningen

Ionization state of the accretion disc in the neutron star low-mass X-ray binary 4U 1728-34

Lyu, Ming; Méndez, Mariano; Zhang, Jian-Fu; Xiang, Fu-Yuan

IMPORTANT NOTE: You are advised to consult the publisher's version (publisher's PDF) if you wish to cite from it. Please check the document version below.

Document Version
Publisher's PDF, also known as Version of record

[Link to publication in University of Groningen/UMCG research database](#)

Ionization state of the accretion disc in the neutron star low-mass X-ray binary 4U 1728–34

Ming Lyu ⬥,[1,2]★ Mariano Méndez,[2] Jian-Fu Zhang[1] and Fu-Yuan Xiang[1]

[1]*Department of Physics, Xiangtan University, Xiangtan, Hunan 411105, China*
[2]*Kapteyn Astronomical Institute, University of Groningen, PO BOX 800, NL-9700 AV Groningen, the Netherlands*

ABSTRACT

We analysed an *XMM–Newton* plus a simultaneous Rossi X-ray Timing Explorer observation and a separate Suzaku observation of the neutron star low-mass X-ray binary 4U 1728–34. We fitted the X-ray spectra with the self-consistent reflection model RELXILL. We found that the inclination angle of 4U 1728–34 is 49 ± 5 degree, consistent with the upper limit of 60 degree deduced from the absence of eclipses or dips in this source. The inclination angle in the fit of the *XMM–Newton*/RXTE observation is larger than 85 degree, which may be due to the possible calibration issues of the PN instrument in timing mode. We also found that the thermal emission from the accretion disc is not significant. This could be explained either by the relatively high column density of the interstellar medium along the line of sight to the source, which decreases the number of soft disc photons, or if most of the soft thermal photons from the disc are reprocessed in the corona. The ionization parameter derived from the fits is larger than the value predicted in the framework of the standard reflection model, wherein the disc is irradiated by an X-ray source above the compact object. This inconsistency suggests that irradiation from the neutron star and its boundary layer may play an important role in the ionization of the accretion disc, and hence in the reflection component in this source.

Key words: accretion, accretion discs – stars: neutron – X-rays: binaries – X-rays: individual: 4U 1728–34.

1 INTRODUCTION

Low-mass X-ray binary systems (LMXBs) consist of a central compact object (a neutron star or a black hole) accreting matter through an accretion disc from a low-mass ($M \leq 1\,M_{\odot}$) donor star. According to the path they trace in an X-ray colour–colour diagram (CD) or hardness-intensity diagram (HID), Hasinger & van der Klis (1989) classified the neutron star LMXBs (NS LMXBs) into two classes, the Atoll and the Z sources. The Z sources (~ 0.5–1 $L_{\rm Edd}$) are brighter than the Atoll sources (0.01–0.2 $L_{\rm Edd}$; e.g. Ford et al. 2000; Done, Gierliński & Kubota 2007; Homan et al. 2007). The Atoll sources display three branches in the CD: the island, the lower, and the upper banana. The branches in the CD correspond to different spectral states, with mass accretion rate increasing from the island (hard spectral state) to the upper banana branch (soft spectral state).

In a typical LMXB system, the emission can be decomposed into the contribution of two main components: (i) A soft, thermal, component due to the emission from the accretion disc and, when appropriate, the neutron star surface and its boundary layer and (ii)

a hard component due to inverse Compton scattering of soft photons from the thermal component(s) by hot electrons in a corona. In the hard spectral state, the inner part of the accretion disc is relatively cool, ~ 0.3–$0.5\,$keV (e.g. Sanna et al. 2013; Lyu et al. 2014), and contributes less than 20 per cent of the total emission between 0.5 and 20 keV. The energy spectrum in the hard state is dominated by a Comptonized component, which is usually described by a power-law-like model with a photon index of $\sim 1.6 - 2.5$ (Yoshida et al. 1993; Méndez et al. 1997). In the truncated disc scenario (e.g. Done et al. 2007, and references therein), the accretion disc in the hard state is truncated far from the central object, thus leading to a relative low inner disc temperature and disc flux, while in the soft spectral state, the soft thermal emission becomes dominant. There are two possible sources of thermal emission in an NS system, either the surface of the NS (plus its boundary layer) or the accretion disc. The disc in the soft state extends down to the inner most stable circular orbit (Shakura & Sunyaev 1973), leading to a high inner disc temperature of $0.7 - 1.0\,$keV (Sanna et al. 2013; Lyu et al. 2014) and a strong thermal component. The electrons in the corona are efficiently cooled down through the inverse Compton scattering process, with seed photons coming from the thermal components. As a consequence, the Comptonized spectrum becomes steep and has a photon index of $\sim 2 - 2.5$ (Miyamoto et al. 1993; Méndez

★ E-mail: lvming@xtu.edu.cn

et al. 1997), and little hard emission is detected in some cases (Gierliński & Done 2003; Zhang et al. 2017).

Many models have been proposed to explain the NS LMXB spectra. Historically, two main types of models were widely used: (i) the 'eastern model' consists of a multitemperature thermal emission from the accretion disc plus a Comptonized component from an optically thin but geometrically thick corona (Mitsuda et al. 1984, 1989) and (ii) the 'western model' consists of a single-temperature blackbody component from the surface of the neutron star (and its boundary layer) and a Comptonized spectrum due to inverse Compton scattering of thermal photons off the hot electrons in the corona (White et al. 1986).

4U 1728–34 was first detected by UHURU scans of the Galactic centre region in 1976 (Forman, Tananbaum & Jones 1976). Later, Lewin, Clark & Doty (1976) and Hoffman et al. (1976) detected type I X-ray bursts from the source, identifying the neutron star nature of the compact object. 4U 1728–34 was classified as an Atoll NS LMXB (Hasinger & van der Klis 1989), at an estimated distance of 4.4−5.1 kpc, deduced from measurements of the peak flux of photospheric radius expansion bursts (Di Salvo et al. 2000; Galloway et al. 2003). Migliari et al. (2003) found a coupling between the disc and the jet in 4U 1728–34 based on a significant correlation between the radio flux density and the X-ray flux. Spectral analysis of 4U 1728–34 has been performed using observations from many satellites in the past, such as Einstein (Grindlay & Hertz 1981), SAS–3 (Basinska et al. 1984), EXOSAT (White et al. 1986), SIGMA (Claret et al. 1994), *ROSAT* (Schulz 1999), BeppoSAX (Di Salvo et al. 2000; Piraino, Santangelo & Kaaret 2000), *ASCA* (Narita, Grindlay & Barret 2001), RXTE, *Chandra* (D'Aí et al. 2006), INTEGRAL (Falanga et al. 2006), *XMM–Newton* (Ng et al. 2010; Egron et al. 2011), BeppoSAX, RXTE (Seifina & Titarchuk 2011), INTEGRAL, RXTE (Tarana et al. 2011), and NuSTAR, Swift (Sleator et al. 2016; Mondal et al. 2017).

In this work, we used an *XMM–Newton* observation plus a simultaneous Rossi X-ray Timing Explorer (RXTE) observation, and a Suzaku observation to explore the spectral properties of 4U 1728–34. We applied full reflection models to investigate the spectral features of the source. Furthermore, we studied the ionization state of the accretion disc by comparing the results from spectroscopy and theory, and we explored the possible mechanisms behind the emission spectrum in this source. The paper is organized as follows: We describe the observations and the details of the data reduction in Section 2. In Sections 3 and 4, we show the spectral analysis process and the results, respectively. Finally, in Section 5 we discuss our findings.

2 OBSERVATIONS AND DATA REDUCTION

In this work, we used data from three satellites: An *XMM–Newton* observation (ObsID:0671180201) plus a simultaneous RXTE observation (ObsID: 96322-01-01-00) taken on 2011-08-28, and a Suzaku observation (ObsID:405048010) obtained on 2010-10-04. We analysed the *XMM–Newton*/RXTE and the Suzaku observation separately in this work.

The *XMM–Newton* observation was taken with the European Photon Imaging Camera, EPIC-PN (Strüder et al. 2001) in timing mode, with a total exposure time of about 52 ks. We used the science analysis system (SAS) version 16.1.0 to reduce the PN data with the latest calibration files. We applied the tool epproc to extract calibrated events, and converted the arrival time of photons to the barycentre of the Solar system using the command barycen. We excluded all events at the edge of a CCD and close to a bad pixel,

and selected only single and double events for the extraction. We estimated the pile-up effect using the command epatplot, as suggested by the SAS thread. When we exclude the central one, three, and five columns, the 0.5–2.0 keV observed-to-model fraction for doubles is 1.050 ± 0.003, 1.022 ± 0.004, and 0.990 ± 0.004, respectively. We finally selected events within a 41-column wide region centred on the source position, excluding the central five columns to eliminate pile up. The EPIC pn spectrum of the full region has a count rate of $\sim 247\,\mathrm{cts\,s^{-1}}$, whereas the one excluding the central five columns has a count rate of $\sim 70\,\mathrm{cts\,s^{-1}}$. We removed all X-ray bursts before we extracted the spectra. For PN timing mode observation, the point spread function (PSF) of the instrument extends further than the CCD boundaries, thus the whole CCD was contaminated by the source photons (Ng et al. 2010; Hiemstra et al. 2011). To model the background, we used the observation of the NS LMXB 4U 1608–52 (ObsID 0074140201) in timing mode when the source was close to quiescence. We excluded the bad time interval with flaring particle background and then extracted the background from a region far from the centre of the PSF (RAWX in [2:5]). We produced the response matrices and ancillary response files (ARFs) with the commands rmfgen and arfgen, respectively. Finally, we rebinned the spectrum with the command specgroup to ensure a minimum of 25 counts in every bin and a maximum oversampling factor of 3.

For the RXTE observation, we used the Proportional Counter Array (PCA; Jahoda et al. 2006) data only since the other instrument, the High Energy X-ray Timing Experiment (HEXTE; Rothschild et al. 1998), was not in a good working condition after 2009. We reduced the data using the HEASOFT package version 6.16 according to the RXTE cook book.[1] We applied the tool saextrct to extract PCA spectra from Standard-2 data, where only the events from the best calibrated detector, PCU2, were selected. We ran the commands pcabackest to generate the PCA background files and pcarsp to produce the response files. Finally, we applied the dead time correction to the spectra.

We used the Suzaku data taken with two instruments onboard: the X-ray imaging spectrometer (XIS) and the hard X-ray detector (HXD). The XIS and HXD detectors cover an energy range of 0.2−12 and 10−70 keV, respectively. The XIS data were collected by two front-illuminated (FI) detectors (XIS0 and XIS3) and one back-illuminated (BI) detector (XIS1). The one-fourth window option and the burst option were applied to the XIS detectors to limit possible pile-up effects.

We followed exactly the steps from the Suzaku Data Reduction Guide[2] to reduce all Suzaku data. We used the tool aepipeline to recalibrate the XIS and HXD events with the latest calibration files, removed bad pixels, and applied the standard GTI selection. After excluding X-ray bursts, we ran the HEASOFT tool xselect to extract XIS spectra from a circular region centred at the position of the source. We found that there was no pile up in the spectra. The redistribution matrix files (RMFs) and ARFs were generated using the tools xisrmfgen and xissimarfgen, respectively. Finally, we used the command addascaspec to combine the spectra of XIS1 and XIS3 to produce the FI spectra. For the HXD–PIN data, we applied the tool hxdpinxbpi to produce the source and background spectra. We applied the dead-time correction to the source spectrum using the pseudo-events files. Since the non-X-ray background (NXB) has a count rate 10 times higher than the real

---

[1]http://heasarc.gsfc.nasa.gov/docs/xte/recipes/cook_book.html
[2]http://heasarc.gsfc.nasa.gov/docs/suzaku/analysis/abc/

background, in order to reduce the Poisson noise, we adjusted the exposure time of the NXB spectra by a factor of 10. Furthermore, a cosmic X-ray background was simulated and added to the NXB to generate a total background spectrum. Finally, we downloaded the response file from the online CALDB according to the Suzaku Data Reduction Guide.

3 SPECTRAL ANALYSIS

In this work, we used XSPEC version 12.10.0 (Arnaud 1996) to fit the PN and PCA spectra together in the $0.9-25$ keV energy range (PN: $0.9-10$ keV; PCA: $10-25$ keV), and the Suzaku spectra in the $1-50$ keV energy range (FI/BI: $1-10$ keV; HXD-PIN: $10-50$ keV). We used the component PHABS to describe the interstellar absorption along the line of sight, with the solar abundance table of Wilms, Allen & McCray (2000) and the photoionization cross-section table of Verner et al. (1996). A multiplicative factor was applied to the model to account for possible calibration difference between different instruments. We fixed this factor to 1 for the PN and FI spectrum, and let it free for the spectrum of the other instruments. Finally, we added a 0.5 per cent systematic error to all the spectra to account for possible effects of the cross calibration on the spectral shape (e.g. Sanna et al. 2013; D'Aì et al. 2015). Next, we describe the models that we fitted to the spectra, and we present the corresponding fitting results in the next section.

3.1 Direct emission

We first tried a thermal component plus a Comptonized component to fit the spectra (e.g. Sleator et al. 2016; Mondal et al. 2017). We selected the model BBODY to describe the thermal emission from the neutron star surface and its boundary layer. For the Comptonized component, we used the thermal Comptonized component NTHCOMP (Zdziarski, Johnson & Magdziarz 1996; Życki, Done & Smith 1999), which describes more accurately the high-energy shape and the low-energy rollover than an exponentially cut-off power-law component. In order to test whether this combination is able to fit the continuum well, we excluded the 5–8 keV energy range where significant residuals caused by iron emission line were present (see Section 3.2 next). We found that the continuum could be well fitted by the BBODY + NTHCOMP model, with a reduced chi-squared value/number of degrees of freedom of 0.99/128 and 1.26/2592 for the *XMM–Newton*/RXTE observation and the Suzaku observation, respectively. We also tried to add the component DISKBB (Mitsuda et al. 1984; Makishima et al. 1986) to fit the possible emission from an accretion disc, and linked the temperature of the accretion disc, $kT_{\rm dbb}$, in the DISKBB component to the seed photon temperature, $kT_{\rm seed}$, in the NTHCOMP component. We found that the additional component DISKBB did not significantly improve the fits: The reduced chi-squared/number of degrees of freedom for the fits were 0.99/127 and 1.21/2591 for the *XMM–Newton*/RXTE and the Suzaku observation, respectively. The DISKBB normalization $N_{\rm dbb}$, in the Suzaku observation in this case became extremely large (208132^{+99428}_{-65410}), which is likely caused by a degeneracy of the parameters in the model. Therefore, we did not use the DISKBB component in the rest-fitting process (see also, Piraino et al. 2000; D'Aí et al. 2006; Seifina & Titarchuk 2011).

The seed photons for the thermal Compton process in the corona could either come from the accretion disc or the neutron star surface and its boundary layer. Sanna et al. (2013) explored the origin of the seed photons by linking the seed photon temperature, $kT_{\rm seed}$, in the NTHCOMP to either the temperature of the accretion disc, $kT_{\rm dbb}$,

in the DISKBB, or the temperature of the neutron star, $kT_{\rm bb}$, in the BBODY, respectively. They found that both options gave statistically acceptable fits, however, the blackbody emission became negligible when linking $kT_{\rm bb}$ in the BBODY to $kT_{\rm seed}$ in the NTHCOMP. We also tried to link $kT_{\rm seed}$ in the NTHCOMP component to the temperature of the neutron star, $kT_{\rm bb}$, however, in this case the fitting became worse and $kT_{\rm bb}$ decreased to ~ 0.33 keV or pegged at the lower boundary 0.3 keV for the *XMM–Newton*/RXTE and the Suzaku observation, respectively. We therefore assumed that the thermal photons from the accretion disc are the seed photons for the Compton process in the corona (e.g. Sanna et al. 2013; Lyu et al. 2014), and we therefore left the parameter $kT_{\rm seed}$ free to vary because, as we explained above, we did not detect the DISKBB component.

3.2 Phenomenological reflection model of the line emission

After fitting the continuum, we found prominent residuals in the iron line region. The existence of residuals around $5-8$ keV in the fits indicates that reflection from the accretion disc may be present therefore we added a GAUSSIAN component to fit the possible iron line emission, constraining the energy of the line to be in the $6.4-6.97$ keV range. We found that the derived GAUSSIAN line profiles were in general broad ($\sigma \sim 0.8$ keV), so we then substituted the GAUSSIAN component with a relativistically broadened LAOR line (Laor 1991) model, which was developed to describe the emission from a line emitted from an accretion disc around a maximally rotating black hole. The parameters of the LAOR component are the emissivity index of the disc, β, the inner and outer radii of the disc, $R_{\rm in}$ and $R_{\rm out}$, respectively, the central energy of the emission line, $E_{\rm line}$, and the inclination angle of the disc with respect to the line of sight, i. We found that the best-fitting parameters did not change significantly when the outer disc radius was fixed at 400 $R_{\rm g}$ compared with the ones when it was free to change. We then fixed the outer disc radius in the model at 400 $R_{\rm g}$, where $R_{\rm g} = GM/c^2$, with G being Newton's constant, c the speed of light, and M the mass of the NS.

3.3 Full reflection models

When X-rays illuminate the accretion disc, the surface of the accretion disc is expected to be ionized, producing a reflection spectrum including fluorescence lines, recombination, and other emissions (e.g. Ross & Fabian 2005). The shape of the reflection spectrum is influenced by the ionization state of the disc, and thus the reflection spectrum is important for understanding the thermal balance of the disc. Therefore, we also fitted the broad-band spectrum with a self-consistent reflection model. We first applied the reflection model RELXILL (García et al. 2014; Dauser et al. 2016), which describes the reflection off the disc illuminated by a power-law source. The RELXILL model combines the relativistic convolution kernel RELCONV (Dauser et al. 2010) with the reflection grid XILLVER (García et al. 2013), and it calculates the reflection spectrum for each emission angle. The fit parameters of the RELXILL model are the inclination of the accretion disc, i, the dimensionless spin parameter, a, the redshift to the source, z, the inner and outer radii of the disc, $R_{\rm in}$ and $R_{\rm out}$, respectively, the inner and outer emissivity index of the accretion disc, $q_{\rm in}$ and $q_{\rm out}$, the breaking radius $R_{\rm br}$ where the emissivity changes, the ionization parameter, ξ, the iron abundance, $A_{\rm Fe}$, the photon index of the power law, Γ, the cut-off energy of the power law, $E_{\rm cut}$, the reflection fraction, $R_{\rm refl}$, and the normalization. We fixed a to 0.17 calculated as $a = 0.47/P_{\rm ms}$ (Braje, Romani & Rauch 2000), where $P_{\rm ms} = 1000/363$ ms (Strohmayer

Table 1. Best-fitting results for the fit to the X-ray spectra of 4U 1728–34 with the phenomenological model. The inclination angle in the *XMM–Newton*/RXTE observation could not be well constrained, so we fixed it to the value in the Suzaku observation when we fit it with the full reflection model (see text). Here, we give the unabsorbed flux (erg cm^{-2} s^{-1}) in the energy range 0.1−100 keV. All errors in the Tables are at the 90 per cent confidence level unless otherwise indicated. A symbol ∗ means that the error pegged at the hard limit of the parameter range.

Model comp	Parameter	Suzaku	*XMM–Newton*/RXTE
PHABS	N_H (10^{22} cm^{-2})	4.84 ± 0.06	4.41 ± 0.21
BBODY	kT_{BB} (keV)	2.2 ± 0.02	2.04 ± 0.03
	Norm (10^{-3})	7.1 ± 0.2	15.1 ± 1.1
	Flux (10^{-10} c.g.s)	6.1 ± 0.2	13.1 ± 0.9
NTHCOMP	Γ	2.23 ± 0.02	2.26 ± 0.06
	kT_e (keV)	7.0 ± 0.3	4.5 ± 0.4
	kT_{bb} (keV)	0.21 ± 0.04	$0.32^{+0.08}_{-0.22*}$
	Norm	0.65 ± 0.03	$1.02^{+0.45}_{-0.17}$
	Flux (10^{-10} c.g.s)	38.7 ± 2.0	$60.6^{+21.1}_{-5.5}$
LAOR	E_{line} (keV)	$6.97^{+0*}_{-0.02}$	6.59 ± 0.07
	β	3.8 ± 0.4	2.46 ± 0.21
	R_{in} (R_g)	6.2 ± 0.7	9.55 ± 3.89
	incl (°)	24.7 ± 1.6	50 (fixed)
	Norm (10^{-3})	1.5 ± 0.2	3.78 ± 0.35
	Flux (10^{-10} c.g.s)	0.15 ± 0.1	0.39 ± 0.03
	χ^2_ν (χ^2/dof)	1.16 (4758/4093)	1.29 (223/172)
	Total flux (10^{-10} c.g.s)	$44.2^{+3}_{-1.6}$	$77.3^{+18.3}_{-8.6}$

et al. 1996) is the spin period of the NS in milliseconds. The inner radius, R_{in}, was set to be larger than 5.44 R_g, while R_{out} and R_{br} were fixed at 400 R_g, and hence q_{in} and q_{out} were linked to vary together. The redshift z was set to zero and A_{Fe} was fixed to the solar abundance.

In order to explore the possible geometry of 4U 1728−34, we also fitted the spectra with another reflection model, RELXILLLP (García et al. 2014; Dauser, García & Wilms 2016). The RELXILLLP model is a relativistic reflection model for the lamppost geometry, which assumes that the corona is located above the accretion disc along the spin axis of the compact object. The RELXILLLP model has the same parameters as RELXILL, but replaces the emissivity indeces and the breaking radius with a new parameter, h, which is the height of the corona. We set the parameter *fixReflFrac* = 0 to fit the reflection freely, and set the rest of the parameters in this model to the same values as in RELXILL.

To sum up, we used the model PHABS∗(BBODY+LAOR + NTH-COMP) to describe the continuum and iron emission line, and the models, PHABS∗(BBODY + RELXILL) and PHABS∗ BBODY + RELX-ILLLP), to model the full reflection spectra. We found that the inclination angle in the *XMM–Newton*/RXTE observation could not be well constrained (it was larger than 85 degree) in the fits, and hence we fixed it at 50 degree, derived from the fits of the full reflection models to the Suzaku observation.
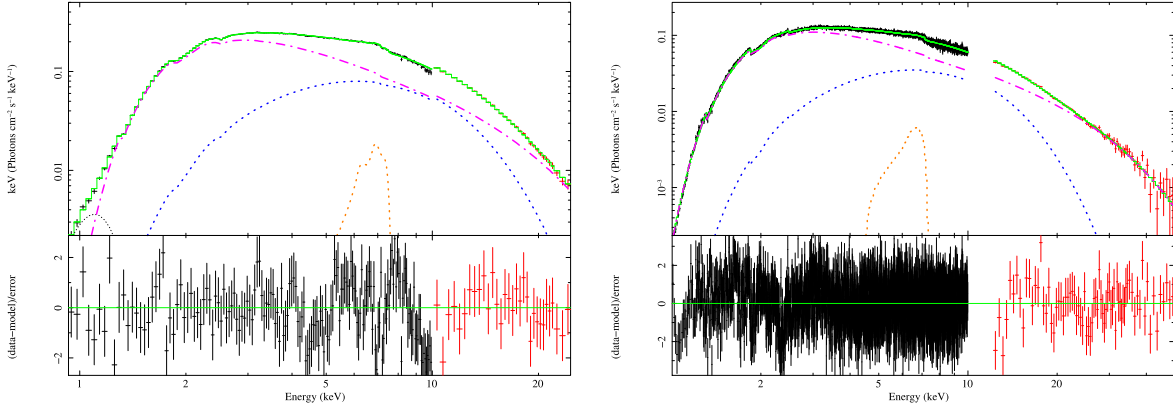
4 RESULTS

In Table 1, we show the fitting results using the LAOR model. The blackbody temperature, kT_{BB}, is 2.2 ± 0.02 keV in the Suzaku observation and 2.04 ± 0.03 keV in the *XMM–Newton*/RXTE observation. The power-law index, Γ, is 2.23 ± 0.02 and 2.26 ± 0.06, while the electron temperature, kT_e, is 7.0 ± 0.3 and 4.5 ± 0.4 keV in the Suzaku and the *XMM–Newton*/RXTE observation, respec-

tively. The corresponding energy of the LAOR line is $6.97^{+0}_{-0.02}$ and 6.59 ± 0.07 keV in the Suzaku and *XMM–Newton*/RXTE observation, respectively, suggesting that the accretion disc is highly or moderately ionized in these two observations. The corresponding spectra, individual components, and residuals of the fits are shown in Fig. 1.

In Table 2, we summarize the fitting results with the reflection model RELXILL. The reduced chi-square with this model is 1.14 and 1.0 for 4094 and 173 degrees of freedom for the Suzaku and *XMM–Newton*/RXTE observation, respectively. The inclination angle was well constrained at 49^{+8}_{-3} degree in the Suzaku observation, consistent with the fact that no eclipse has ever been observed in this source. The reflection fraction, R_{refl}, is 0.54 ± 0.08 in the Suzaku observation and $1.39^{+0.6}_{-0.32}$ in the *XMM–Newton*/RXTE observation. This may suggest that more photons from the corona illuminate the accretion disc in the *XMM–Newton*/RXTE than in the Suzaku observation, which is also consistent with the higher ionization state of the disc in the *XMM–Newton*/RXTE observation. The ionization parameter, $log(\xi)$, is 2.71 ± 0.07 in the Suzaku observation, and 3.92 ± 0.16 in the *XMM–Newton*/RXTE observation. The inner radius of the disc, R_{in}, is $14.1^{+10.7}_{-2.9}$ and $5.44^{+2.32}_{-0}$ R_g in the Suzaku and *XMM–Newton*/RXTE observation, respectively.

We show the fitting results with the reflection model RELXILLLP in Table 3. Most of the parameters in the fits with the model RELXILLLP are similar to the ones in the fit with RELXILL, except that the reflection fraction, R_{refl}, is systematically higher in RELXILLLP than in RELXILL. In the case of RELXILLLP, R_{refl} is $1.68^{+1.19}_{-0.33}$ and $3.05^{+1.11}_{-0.65}$ in the Suzaku and *XMM–Newton*/RXTE observation, respectively. There is no clear difference in the height of the corona, h, in the two observations: h is $15.5^{+11.8}_{-9.2}$ R_g (90 per cent confidence level) in the Suzaku observation, while it is 22.3 ± 6.7 R_g in the *XMM–Newton*/RXTE observation. The corresponding spectra, individual components, and residuals of the fits are shown in Fig. 2.

Figure 1. Fitting results with the phenomenological reflection model PHABS∗(BBODY+NTHCOMP + LAOR) for the *XMM–Newton*/RXTE (left) and the Suzaku (right) observations of 4U 1728–34. Each plot shows the fitted spectra and the individual model components (main panel), and the residuals in terms of sigmas (sub panel). The component BBODY, NTHCOMP, LAOR, and the sum of all these model components are plotted with a blue dotted, magenta dash–dotted, yellow dotted line and green line, respectively. Since the FI and BI spectra in the Suzaku observation are mostly on top of each other in the plot, here we do not plot the BI spectra for clarity. The residuals in the plots are rebinned for plotting purposes.

Table 2. Best-fitting results for the fit to the X-ray spectra of 4U 1728–34 with the reflection model PHABS∗(BBODY + RELXILL). We fixed the inclination angle in the *XMM–Newton*/RXTE observation to the value in the Suzaku observation since this parameter in the *XMM–Newton*/RXTE observation could not be well constrained. Here, we give the unabsorbed flux (erg cm^{-2} s^{-1}) in the energy range $0.1-100$ keV. A symbol ∗ means that the error pegged at the hard limit of the parameter range.

| Model Comp	Parameter	Suzaku	*XMM–Newton*/RXTE
PHABS	$N_{\rm H}$ (10^{22} cm^{-2})	4.92 ± 0.03	5.18 ± 0.14
BBODY	$kT_{\rm BB}$ (keV)	2.27 ± 0.04	2.15 ± 0.03
	Norm (10^{-3})	6.9 ± 0.2	19.4 ± 0.5
	Flux (10^{-10} c.g.s)	5.4 ± 0.1	$16.2^{+0.7}_{-0.2}$
RELXILL	β	$2.8^{+0.5}_{-0.2}$	2.32 ± 0.16
	incl (°)	49^{+8}_{-3}	50 (fixed)
	$R_{\rm in}$ ($R_{\rm g}$)	$14.1^{+10.7}_{-2.9}$	$5.44^{+2.32}_{-0*}$
	Γ	2.03 ± 0.04	2.43 ± 0.09
	$\log(\xi)$	2.71 ± 0.07	3.92 ± 0.16
	$E_{\rm cut}$ (keV)	16.6 ± 1.2	$19.95^{+7.03}_{-2.0}$
	$R_{\rm refl}$	0.54 ± 0.08	$1.39^{+0.6}_{-0.32}$
	Norm (10^{-3})	5.5 ± 0.3	9.3 ± 2.4
	Flux (10^{-10} c.g.s)	$66.7^{+2.8}_{-1.5}$	206^{+65}_{-19}
	χ^2_ν (χ^2/degrees of freedom)	1.14 (4668/4094)	1.0 (173/173)
	Total flux (10^{-10} c.g.s)	$73.6^{+1.5}_{-3}$	222^{+66}_{-19}

5 DISCUSSION

Egron et al. (2011) analysed one *XMM–Newton* observation of 4U 1728–34 with a reflection model and constrained the inclination angle of the system to be within 44–60 degree. Mondal et al. (2017) analysed two simultaneous NuSTAR and Swift observations of 4U 1728–34 and constrained the inclination angle to be within 22–40 degree. In this work, we find that the inclination angle of 4U 1728–34 is about 49 ± 5 degree from the fit to the Suzaku observation, consistent with the range from Egron et al. (2011) but a bit larger than the value of Mondal et al. (2017). We also found that the inclination angle is larger than 85 degree and could not be well constrained with the *XMM–Newton*/RXTE data, similar to previous findings (e.g. Pandel, Kaaret & Corbel 2008; Sanna et al. 2013). Sanna et al. (2013) analysed another NS LMXB 4U 1636–53 using six *XMM–Newton* observations with the PN camera in timing mode,

plus simultaneous RXTE observations, and found high inclination angles in the fits, inconsistent with the absence of eclipses and dips in 4U 1636–53. They suggested that the PN timing mode data may be affected by calibration issues, which leads to high inclination angles in the fits. In this work, the derived high inclination angles in the *XMM–Newton*/RXTE observation may be due to the same calibration issues. When we fit the *XMM–Newton* spectrum alone, the inclination angle is still larger than 85 degree. The problem with the calibration of EPIC instrument would lead to a steeper spectrum, and hence to a higher inclination angle in the fits.

The fitting results show that the NTHCOMP component dominated the broad-band energy spectrum in both the *XMM–Newton*/RXTE and Suzaku observations. This agrees with the conclusion of Seifina & Titarchuk (2011) that the energy spectrum of 4U 1728–34 in all states is dominated by the power-law component. Seifina & Titarchuk (2011) investigated more than 120 RXTE observations of

Table 3. Best-fitting results for the fit to the X-ray spectra of 4U 1728–34 with the reflection model PHABS∗(BBODY + RELXILLLP). We fixed the inclination angle in the *XMM–Newton*/RXTE observation to the value in the Suzaku observation since this parameter in the *XMM–Newton*/RXTE observation could not be well constrained. Here, we give the unabsorbed flux (erg cm^{-2} s^{-1}) in the energy range $0.1-100$ keV. A symbol ∗ means that the error pegged at the hard limit of the parameter range.

Model comp	Parameter	Suzaku	*XMM–Newton*/RXTE
PHABS	$N_{\rm H}(10^{22}\,{\rm cm}^{-2})$	4.91 ± 0.03	5.17 ± 0.12
BBODY	$kT_{\rm BB}({\rm keV})$	2.27 ± 0.03	2.15 ± 0.02
	Norm (10^{-3})	6.9 ± 0.2	19.4 ± 0.4
	Flux $(10^{-10}$ c.g.s)	6.0 ± 0.2	$16.2^{+0.7}_{-0.4}$
RELXILLLP	h $(R_{\rm g})$	$15.5^{+11.8}_{-9.2}$	22.3 ± 6.7
	incl (degree)	49^{+6}_{-3}	50 (fixed)
	$R_{\rm in}(R_{\rm g})$	$13.8^{+8.7}_{-3.0}$	$5.44^{+3.87}_{-0*}$
	Γ	2.04 ± 0.04	2.43 ± 0.10
	$\log(\xi)$	2.7 ± 0.06	3.91 ± 0.15
	$E_{\rm cut}$ (keV)	16.6 ± 0.8	$19.2^{6.3}_{-1.8}$
	$R_{\rm refl}$	$1.68^{+1.19}_{-0.33}$	$3.05^{+1.11}_{-0.65}$
	Norm (10^{-3})	$7.2^{+3.8}_{-1.2}$	11.8 ± 3.0
	Flux $(10^{-10}$ c.g.s)	$64.6^{+2.8}_{-3.8}$	204^{+43}_{-25}
	$\chi^2_\nu(\chi^2$/degrees of freedom)	1.14 (4669/4094)	1.04 (180/173)
	Total flux $(10^{-10}$ c.g.s)	70.8 ± 3.1	220^{+41}_{-17}
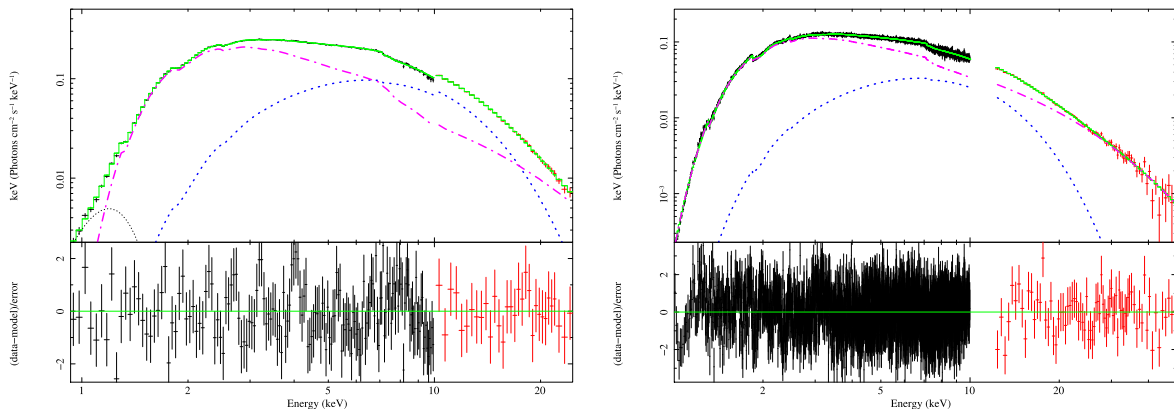
Figure 2. Fitting results with the full reflection model PHABS∗(BBODY + RELXILLLP) for the *XMM–Newton*/RXTE (left) and the Suzaku (right) observations of 4U 1728–34. Each plot shows the fitted spectra and the individual model components (main panel), and the residuals in terms of sigmas (subpanel). The component BBODY, RELXILLLP, and the sum of the model components are plotted with a blue dotted, magenta dash–dotted, and green line, respectively. Since the FI and BI spectra in the Suzaku observation are mostly on top of each other in the plot, here we do not plot the BI spectra for clarity. The residuals in the plots are rebinned for plotting purposes.

4U 1728–34, and they found that most of the soft thermal emission from the accretion disc in 4U 1728–34 is reprocessed in the corona, thus the direct disc emission is weak. In this work, the thermal emission from the disc in both the *XMM–Newton*/RXTE and the Suzaku observation is not required, consistent with their finding. A further calculation shows that the upper limit of the weak DISKBB component in the fit in this work is able to produce the observed Comptonized component. The absence of the disc emission can also be the consequence of the relatively high column density, $N_{\rm H}$, of the interstellar medium along the line of sight to the source, which reduces the number of soft disc photons that we observe, thus leading to a weak disc component in the observed energy spectra.

Ballantyne (2017) investigated the ionization parameter in the accretion disc at a radius r from the black hole, with the disc being irradiated by an X-ray source at a height, h, above the black hole

symmetry axis. Ballantyne (2017) developed a formula that takes into account the effects of gravitational light-bending and focusing of radiation on to the disc. According to their calculation, there is a strong ionization gradient across the surface of the inner disc that depends on the black hole spin and the lamppost height. This model provides a good way to connect the height of the corona with the ionization state and the inner radius of the accretion disc. For this, we applied equation (10) in Ballantyne (2017):

$$\xi(r, h) = (5.44 \times 10^{10}) \left(\frac{\eta}{0.1}\right)^{-2} \left(\frac{\alpha}{0.1}\right) \lambda^3 \left(\frac{r}{r_{\rm g}}\right)^{-3/2} R_z^{-2} R_T^{-1}$$
$$\times R_R^3 f(1 - f)^3 F(r, h) g_{\rm lp}^2 \mathcal{A}^{-1} {\rm erg\ cm\ s}^{-1}, \tag{1}$$

where $\xi(r, h)$ is the ionization parameter of the disc at a radius r from the central source where the illuminating lamppost is at a height h, η is the radiative efficiency of the accretion process, α is the viscosity
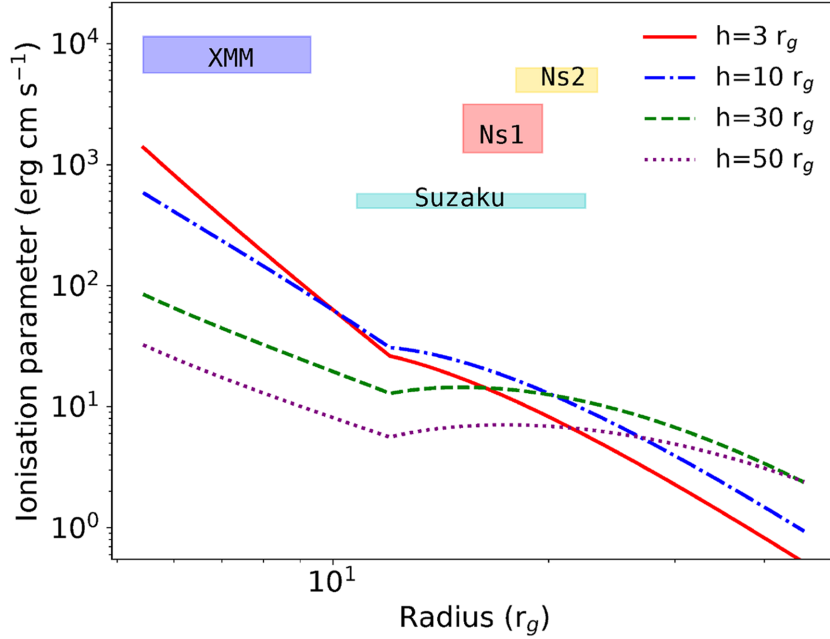
Figure 3. The predicted ionization profiles of an accretion disc illuminated by a lamppost X-ray source located at different heights above the central source. The curves are calculated using equation (1) in the text, taken from Ballantyne (2017), assuming $\eta = 0.1$, $\alpha = 0.3$, $\lambda = 0.2$, and $f = 0.45$. The spin parameter is fixed at 0.17 for 4U 1728–34 and r_{in} and r_{out} are 5.44 and 400 R_g, respectively. The R_R, R_z, and R_T factors at $r < 12 R_g$ are fixed at their values at $r = 12 R_g$ to avoid an unphysical break in $\xi(r, h)$. As shown in the legend, ionization profiles at different heights are marked in different line styles and colours. Here, we compared the predicted ionization profiles with the ionization derived in this work and in Mondal et al. (2017). The two observations in this work were labelled as *XMM–Newton* and Suzaku, and the two simultaneous NuSTAR and Swift observations in Mondal et al. (2017) were labelled as Ns1 and Ns2, respectively.

parameter, λ is the Eddington ratio, $\lambda = L_{bol}/L_{Edd}$, R_R, R_z, and R_T are relativistic corrections to the Newtonian α-disc equations (Krolik 1999), f is the coronal dissipation fraction, and $g_{lp} = \nu_{disc}/\nu_{src}$ is the ratio between the measured frequency of a photon striking the disc and its frequency at the source (Dauser et al. 2013). The function $F(r, h)$ in the equation describes the shape of the irradiation pattern (Fukumura & Kazanas 2007), and $\mathcal{A}$ is the integral of $F(r, h) \times g_{lp}^2$ over the entire disc, $\mathcal{A} = \int_{r_{in}}^{r_{out}} F(r, h) g_{lp}^2 dS(r)$.

For the calculations, we set the $\eta = 0.1$, $\alpha = 0.3$ (Penna et al. 2013; Ballantyne 2017), $\lambda = 0.2$, and $f = 0.45$ (Vasudevan & Fabian 2007). The spin parameter, a, is fixed at 0.17 for 4U 1728–34 and r_{in} and r_{out} are 5.44 and 400 R_g, respectively. We found that there was a break of the ionization profiles around $r = 12 R_g$, similar to the one at $r = 4 R_g$ reported in the simulation of a fast-rotating black hole system in Ballantyne (2017). This break is due to the divergence of R_R and R_T as the radius approaches the innermost stable circular orbit. We then applied the same procedure as in Ballantyne (2017) to fix this: the (R_R, R_z, R_T) factors at $r < 12 R_g$ are fixed at their values at $r = 12 R_{1Å}$.

Fig. 3 shows the ionization profiles when the illuminating corona is located at different heights above the disc. We compared the ionization curves predicted by the formula with the values derived from the fits with the model RELXILLLP in this work and the ones from the fits with the model RELXILL to two simultaneous NuSTAR and Swift observations in Mondal et al. (2017). As shown in the figure, the ionization profiles predicted by the model of Ballantyne (2017) are significantly smaller than the range derived from the observations. The ionization parameter is below 100 at $r > 10 R_g$, while it increases rapidly as the radius further decreases but is still lower than the range from the fits.

The difference between the ionization parameter predicted by the model and the one deduced from data can be bridged if we changed

the value of certain parameters in the model. Notwithstanding, the new values that the parameters must take for the model to qualitatively match the data either contradict some observational result, or are unphysical. For instance, for the model to match the data, the luminosity of the source should be 40 per cent of the Eddington luminosity, $\lambda = 0.4$ in equation (1), whereas the spectral fits indicate that the luminosity in this observation was about 20 per cent Eddington. To make it 40 per cent Eddington, either the mass of the NS needs to be 0.7 $M_\odot$ or the distance should be as large as 7 kpc, which is inconsistent with previous observational results. For instance, Di Salvo et al. (2000) showed that the distance to 4U 1728–34 is about 5.1 kpc assuming a 1.4 $M_\odot$ NS. Galloway et al. (2003) derived a distance of 4.4 (4.8) kpc for a M = 1.4 (2.0) $M_\odot$ NS with cosmic atmospheric abundance (X = 0.7), while the distance could be up to 30 per cent larger ($\sim$6.2 kpc) if the atmosphere of the NS consisted purely of helium. The model would also match the data if we increased the viscosity parameter, α, from 0.3 to 1, or decreased the radiative efficiency from 0.1 to 0.03, however, in these cases the adopted values of the parameters deviate significantly from the values deduced in previous work. Typically $\alpha \sim 0.1$ (e.g. Frank, King & Raine 2002), whereas some work yields even smaller values of this parameter. For example, in the black hole candidate GRS 1915 + 105, Belloni et al. (1997) found that the viscosity parameter is only 0.000 04 and 0.0005 for the Schwarzschild and extreme Kerr cases, respectively.

The inconsistency between the ionization parameter predicted by the model and the ones obtained from the fits may be due to the fact that the disc is also illuminated by radiation from the NS and its boundary layer, which is not included in the standard reflection models. Cackett et al. (2010) investigated the iron emission lines in 10 NS LMXBs, and found that illuminating photons likely come from the NS and the boundary layer. Their

analysis showed that the spectra could be well fitted with a reflection model, with the accretion disc being illuminated by the blackbody component. Besides, they further calculated the maximum height of the boundary layer, $z < 24$ km, consistent with the scenario that the boundary layer illuminates a geometrically thin disc. A subsequent analysis of the bright atoll source 4U 1705–44 by D'Aì et al. (2010) also showed that the spectrum could be well fitted by the sum of two thermal components together with a reflection component, wherein the blackbody component provides illuminating photons to the disc. Their analysis provides another example that the reflection component in NS LMXBs may come from hard X-ray thermal irradiation, which is likely to be the emission from the boundary layer.

There were several type I X-ray bursts in the observations processed in this work, and hence the burst emission may also illuminate and ionize the accretion disc. Ballantyne (2004) presented models of X-ray reflection from a constant-density slab illuminated by a blackbody emitted from an NS burst. The simulated spectral showed a prominent Fe line, while the reflection profiles drop off quickly above 10 keV compared to the profiles assuming power-law component illumination. Nevertheless, as calculated in Ballantyne & Strohmayer (2004), the recombination time for He-like Fe (Fe XXV) is only $\sim 10^{-4}$ s, so the disc will soon return to its previous ionization state after a burst. Therefore, the bursts will likely have no or little contribution to the average ionization state of the disc.

6 SUMMARY

In this work, we used an *XMM–Newton* plus simultaneous RXTE observation and a Suzaku observation to study the spectral properties of the NS LMXB 4U 1728–34. We found that the spectra could be well fitted with a model that does not include thermal emission from the accretion disc. The continuum is dominated by the hard component, while both the full reflection models – RELXILL and RELXILLLP – provide good fits to the spectra. The inclination angle of 4U 1728–34 derived from the Suzaku observation is 49 ± 5 degree, while it is not well constrained in the *XMM–Newton*/RXTE observation. The accretion disc is moderately to highly ionized in these two observations, with the illuminating source located at similar heights in the Suzaku and *XMM–Newton*/RXTE observation. We found that the ionization parameter derived in this work and in Mondal et al. (2017) are larger than, and inconsistent with, the ones predicted by the lamppost model of Ballantyne (2017), assuming that the disc is irradiated only by an X-ray source above the compact object. This inconsistency may be due to the effect of the contribution from the NS and its boundary layer to the reflected emission, which is not included in the model. A model focusing on the roles of both the NS (its boundary layer) and the corona in the illuminating and ionizing process is needed to investigate NS LMXBs; in the meantime, high-quality data from observations is also required in order to break possible degeneracy problems in the spectral analysis.

REFERENCES

Arnaud K. A., 1996, in Jacoby G. H., Barnes J., eds, ASP Conf. Ser. Vol. 101, Astronomical Data Analysis Software and Systems V . Astron. Soc. Pac., San Francisco, p. 17
Ballantyne D. R., 2004, MNRAS, 351, 57
Ballantyne D. R., 2017, MNRAS, 472, L60
Ballantyne D. R., Strohmayer T. E., 2004, ApJ, 602, L105
Basinska E. M., Lewin W. H. G., Sztajno M., Cominsky L. R., Marshall F. J., 1984, ApJ, 281, 337
Belloni T., Méndez M., King A. R., van der Klis M., van Paradijs J., 1997, ApJ, 488, L109
Braje T. M., Romani R. W., Rauch K. P., 2000, ApJ, 531, 447
Cackett E. M. et al., 2010, ApJ, 720, 205
Claret A. et al., 1994, ApJ, 423, 436
D'Aí A. et al., 2006, A&A, 448, 817
D'Aì A. et al., 2010, A&A, 516, A36
D'Aì A. et al., 2015, MNRAS, 449, 4288
Dauser T., Wilms J., Reynolds C. S., Brenneman L. W., 2010, MNRAS, 409, 1534
Dauser T., Garcia J., Wilms J., Böck M., Brenneman L. W., Falanga M., Fukumura K., Reynolds C. S., 2013, MNRAS, 430, 1694
Dauser T., García J., Walton D. J., Eikmann W., Kallman T., McClintock J., Wilms J., 2016, A&A, 590, A76
Dauser T., García J., Wilms J., 2016, Astron. Nachr., 337, 362
Di Salvo T., Iaria R., Burderi L., Robba N. R., 2000, ApJ, 542, 1034
Done C., Gierliński M., Kubota A., 2007, A&AR, 15, 1
Egron E. et al., 2011, A&A, 530, A99
Falanga M., Götz D., Goldoni P., Farinelli R., Goldwurm A., Mereghetti S., Bazzano A., Stella L., 2006, A&A, 458, 21
Ford E. C., van der Klis M., Méndez M., Wijnands R., Homan J., Jonker P. G., van Paradijs J., 2000, ApJ, 537, 368
Forman W., Jones C., Tananbaum H., 1976, ApJ, 206, L29
Frank J., King A., Raine D. J., 2002, Accretion Power in Astrophysics , 3rd edn. Cambridge Univ. Press, Cambridge
Fukumura K., Kazanas D., 2007, ApJ, 664, 14
Galloway D. K., Psaltis D., Chakrabarty D., Muno M. P., 2003, ApJ, 590, 999
García J. et al., 2014, ApJ, 782, 76
García J., Dauser T., Reynolds C. S., Kallman T. R., McClintock J. E., Wilms J., Eikmann W., 2013, ApJ, 768, 146
Gierliński M., Done C., 2003, MNRAS, 342, 1083
Grindlay J. E., Hertz P., 1981, ApJ, 247, L17
Hasinger G., van der Klis M., 1989, A&A, 225, 79
Hiemstra B., Méndez M., Done C., Díaz Trigo M., Altamirano D., Casella P., 2011, MNRAS, 411, 137
Hoffman J. A., Lewin W. H. G., Doty J., Hearn D. R., Clark G. W., Jernigan G., Li F. K., 1976, ApJ, 210, L13
Homan J. et al., 2007, ApJ, 656, 420
Jahoda K., Markwardt C. B., Radeva Y., Rots A. H., Stark M. J., Swank J. H., Strohmayer T. E., Zhang W., 2006, ApJS, 163, 401
Krolik J. H., 1999, Active galactic nuclei : from the central black hole to the galactic environment. Princeton Univ. Press, Princeton, NJ
Laor A., 1991, ApJ, 376, 90
Lewin W. H. G., Clark G., Doty J., 1976, in Marsden B. G., ed, IAU Circ., No. 2922, #1
Lyu M., Méndez M., Sanna A., Homan J., Belloni T., Hiemstra B., 2014, MNRAS, 440, 1165
Makishima K., Maejima Y., Mitsuda K., Bradt H. V., Remillard R. A., Tuohy I. R., Hoshi R., Nakagawa M., 1986, ApJ, 308, 635

Méndez M., van der Klis M., van Paradijs J., Lewin W. H. G., Lamb F. K., Vaughan B. A., Kuulkers E., Psaltis D., 1997, ApJ, 485, L37

Migliari S., Fender R. P., Rupen M., Jonker P. G., Klein-Wolt M., Hjellming R. M., van der Klis M., 2003, MNRAS, 342, L67

Mitsuda K. et al., 1984, PASJ, 36, 741

Mitsuda K., Inoue H., Nakamura N., Tanaka Y., 1989, PASJ, 41, 97

Miyamoto S., Iga S., Kitamoto S., Kamado Y., 1993, ApJ, 403, L39

Mondal A. S., Pahari M., Dewangan G. C., Misra R., Raychaudhuri B., 2017, MNRAS, 466, 4991

Narita T., Grindlay J. E., Barret D., 2001, ApJ, 547, 420

Ng C., Díaz Trigo M., Cadolle Bel M., Migliari S., 2010, A&A, 522, A96

Pandel D., Kaaret P., Corbel S., 2008, ApJ, 688, 1288

Penna R. F., Sądowski A., Kulkarni A. K., Narayan R., 2013, MNRAS, 428, 2255

Piraino S., Santangelo A., Kaaret P., 2000, A&A, 360, L35

Ross R. R., Fabian A. C., 2005, MNRAS, 358, 211

Rothschild R. E. et al., 1998, ApJ, 496, 538

Sanna A., Hiemstra B., Méndez M., Altamirano D., Belloni T., Linares M., 2013, MNRAS, 432, 1144

Schulz N. S., 1999, ApJ, 511, 304

Seifina E., Titarchuk L., 2011, ApJ, 738, 128

Shakura N. I., Sunyaev R. A., 1973, A&A, 24, 337

Sleator C. C. et al., 2016, ApJ, 827, 134

Strohmayer T. E., Zhang W., Swank J. H., Smale A., Titarchuk L., Day C., Lee U., 1996, ApJ, 469, L9

Strüder L. et al., 2001, A&A, 365, L18

Tarana A., Belloni T., Bazzano A., Méndez M., Ubertini P., 2011, MNRAS, 416, 873

Vasudevan R. V., Fabian A. C., 2007, MNRAS, 381, 1235

Verner D. A., Ferland G. J., Korista K. T., Yakovlev D. G., 1996, ApJ, 465, 487

White N. E., Peacock A., Hasinger G., Mason K. O., Manzo G., Taylor B. G., Branduardi-Raymont G., 1986, MNRAS, 218, 129

Wilms J., Allen A., McCray R., 2000, ApJ, 542, 914

Yoshida K., Mitsuda K., Ebisawa K., Ueda Y., Fujimoto R., Yaqoob T., Done C., 1993, PASJ, 45, 605

Zdziarski A. A., Johnson W. N., Magdziarz P., 1996, MNRAS, 283, 193

Zhang G., Méndez M., Sanna A., Ribeiro E. M., Gelfand J. D., 2017, MNRAS, 465, 5003

Życki P. T., Done C., Smith D. A., 1999, MNRAS, 309, 561

This paper has been typeset from a TEX/LATEX file prepared by the author.